2008

Single spin Toffoli-Fredkin logic gate

Amit Ranjan Trivedi
Virginia Commonwealth University

S. Bandyopadhyay
Virginia Commonwealth University, sbandy@vcu.edu

Trivedi, A. R., and Bandyopadhyay, S. Single spin Toffoli-Fredkin logic gate. Journal of Applied Physics, 103, 104311 (2008).

Single spin Toffoli–Fredkin logic gate

Amit Ranjan Trivedi and S. Bandyopadhyay[a)]
Department of Electrical and Computer Engineering, Virginia Commonwealth University, Richmond, Virginia 23284, USA

(Received 22 June 2007; accepted 4 April 2008; published online 29 May 2008)

The Toffoli–Fredkin (TF) gate is a universal reversible logic gate capable of performing logic operations without dissipating energy. Here, we show that a linear array of three quantum dots, each hosting a single electron, can realize the TF gate, if we encode logic bits in the spin polarization of the electrons and allow nearest neighbor exchange coupling. The dynamics of the TF gate is realized by selectively driving spin resonances in the coupled spin system with an ac magnetic field. The conditions for gate operation are established, and an estimate of the switching speed and gate error are provided. © *2008 American Institute of Physics*. [DOI: 10.1063/1.2937200]

I. INTRODUCTION

The Toffoli–Fredkin (TF) gate is a universal classical reversible logic gate[1] that can be switched without dissipating energy.[2] This makes it attractive for low-power and/or high density logic circuits.

The TF gate has three inputs (A,B,C) and three outputs (A',B',C'). A and B are the so-called control bits and C is the target bit. The output-input relations are

$$A' = A,$$

$$B' = B,$$

$$C' = (A \cdot B) \oplus C,$$

where $\cdot$ denotes the Boolean AND and $\oplus$ denotes the Boolean XOR operations. In other words, $C' = \bar{C}$ if $A=B=1$ and $C'=C$ otherwise. If we can realize these input-output relations, we will have realized the TF gate.

The feasibility of implementing reversible logic operations in generic spin based systems have been discussed many times in different contexts,[3–6] but without any concrete scheme. More recently, there has been a spate of activity in realizing quantum computers with spins in NMR systems[7] and, more importantly, in semiconductor quantum dots.[8–12] Unlike NMR based schemes, the quantum dot based schemes are scalable and hence more attractive. These schemes do not specifically address the TF gate but rather arbitrary unitary (reversible) operations on spin, which, of course, can be ultimately configured to implement a TF gate. Here, we propose a direct and concrete scheme for the realization of the TF gate with coupled spins. It is based on the selective driving of resonances that is often used for reversible logic operations in other (nonspin) systems.[13–15]

II. THE SINGLE SPIN TF GATE

The TF gate is realized with a linear array of three exchange coupled spins, each housed in a quantum dot. The entire array is placed in a global dc magnetic field. The spin polarization in any dot can be either parallel or antiparallel to this global field. No other spin polarization is stable since it will not be an eigenstate of the Hamiltonian.

The three-dot array is shown in Fig. 1. The quantum mechanical wavefunctions of electrons in nearest neighbor dots overlap in space causing exchange coupling between them. We will assume that the "upspin" state (aligned antiparallel to the global magnetic field) encodes the classical logic bit 1 and the "downspin" state (parallel to the global field) encodes bit 0.

We will regard the spin polarizations in the three dots as the output bits A', B', and C' at any time. Since $A'=A$ and $B'=B$, inputs can be provided directly to the peripheral dots **A** and **B** by orienting the spins in these dots along chosen directions with local magnetic fields generated by inductors, so that they conform to the control bits A and B. We will now find the spin polarizations in dot **C**. To prove the dynamics of the TF gate, we merely have to show that C toggles if $A=B=1$, and nothing happens otherwise. This will be shown next.

If the charging energy (intradot Coulomb repulsion) within each dot is sufficiently strong, then at half-filling (one electron per dot), the three-spin array in Fig. 1 can be described by the Heisenberg Hamiltonian,[16]

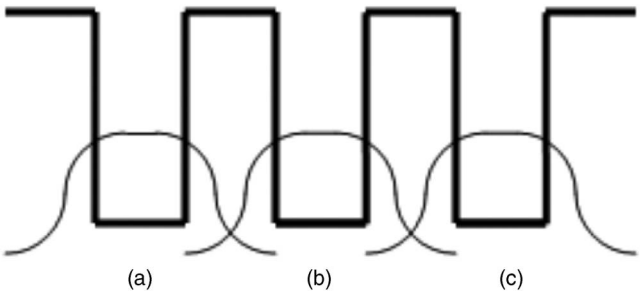

FIG. 1. Potential profile of three exchange coupled quantum dots. Wavefunctions of nearest neighbors overlap causing exchange coupling between them.

[a)]Author to whom correspondence should be addressed. Electronic mail: sbandy@vcu.edu.

$$H_{\text{Heisenberg}} = \sum_{\langle ij \rangle} J_{ij}^{\parallel} \sigma_{zi}\sigma_{zj} + \sum_{\langle ij \rangle} J_{ij}^{\perp}(\sigma_{xi}\sigma_{xj} + \sigma_{yi}\sigma_{yj}) + \sum_{\text{input dots}} \sigma_{zi} h_{zi}^{\text{inputs}} + \sum_{i} \sigma_{zi} h_{zi}^{\text{global}},$$

where the σs are Pauli spin matrices. We adopt the convention that the direction of the global magnetic field, as well as the local magnetic fields writing input data in dots **A** and **B**, is the z direction. Therefore, the last two terms above account for the Zeeman energies associated with these magnetic fields. The first two terms account for the exchange interaction between nearest neighbors (the angular brackets denote nearest neighbors). We will assume the isotropic case whereby $J_{ij}^{\perp} = J_{ij}^{\parallel} = J$, where J is the exchange energy, which is nonzero if the wavefunctions in dots i and j overlap in space.

If we designate the upspin and downspin states as $\uparrow$ and $\downarrow$ respectively, then the three-spin basis states representing the spin configurations in the three-dot array are $|\downarrow\downarrow\downarrow\rangle$, $|\downarrow\downarrow\uparrow\rangle$, $|\downarrow\uparrow\downarrow\rangle$, $|\downarrow\uparrow\uparrow\rangle$, $|\uparrow\downarrow\downarrow\rangle$, $|\uparrow\downarrow\uparrow\rangle$, $|\uparrow\uparrow\downarrow\rangle$, $|\uparrow\uparrow\uparrow\rangle$, where the first entry is the spin polarization in dot **A**, the second in dot **C**, and the third in dot **B**. These eight basis functions form a complete orthonormal set. The matrix elements $\langle \phi_m | H_{\text{Heisenberg}} | \phi_n \rangle$ are given in the matrix below, where the $\phi_{m,n}$ are the three-electron basis states enumerated above,

$$\begin{pmatrix}
2J - h_A - h_B - 3Z & 0 & 0 & 0 & 0 & 0 & 0 & 0 \\
0 & -h_A + h_B - Z & 2J & 0 & 0 & 0 & 0 & 0 \\
0 & 2J & -2J - h_A - h_B - Z & 0 & 2J & 0 & 0 & 0 \\
0 & 0 & 0 & -h_A + h_B + Z & 0 & 2J & 0 & 0 \\
0 & 0 & 2J & 0 & h_A - h_B - Z & 0 & 0 & 0 \\
0 & 0 & 0 & 2J & 0 & -2J + h_A + h_B + Z & 2J & 0 \\
0 & 0 & 0 & 0 & 0 & 2J & h_A - h_B + Z & 0 \\
0 & 0 & 0 & 0 & 0 & 0 & 0 & 2J + h_A + h_B + 3Z
\end{pmatrix}.$$

In the above matrix, Z is one-half of the Zeeman splitting energy associated with the global magnetic field, while $2h_A$ and $2h_B$ are the Zeeman splitting energies in dots **A** and **B** caused by the local magnetic fields that write control bits A and B. If the local magnetic field is in the direction of the global magnetic field (downspin direction) and writes bit 0, then the corresponding h is positive; otherwise, it is negative. The quantity J is always positive.

We will evaluate the eight eigenenergies E_n $(n=1-8)$ by finding the eigenvalues of the 8×8 matrix above and the corresponding eigenstates,

$$\psi_n = c_1^n|\downarrow\downarrow\downarrow\rangle + c_2^n|\downarrow\downarrow\uparrow\rangle + c_3^n|\downarrow\uparrow\downarrow\rangle + c_4^n|\downarrow\uparrow\uparrow\rangle + c_5^n|\uparrow\downarrow\downarrow\rangle + c_6^n|\uparrow\downarrow\uparrow\rangle + c_7^n|\uparrow\uparrow\downarrow\rangle + c_8^n|\uparrow\uparrow\uparrow\rangle = [c_1^n, c_2^n, c_3^n, c_4^n, c_5^n, c_6^n, c_7^n, c_8^n].$$

This exercise will be repeated for four cases, $h_A = \pm h$ and $h_B = \pm h$, which correspond to the four possible control bit combinations $(A=1,0$ and $B=1,0)$.

Case I: $h_A = h_B = h$: This is the case when $A=B=0$.

The eigenenergies and eigenstates corresponding to this case are shown in Table I. The eigenenergies are arranged in ascending order (i.e., the first entry is the ground state and the last entry is the highest excited state), *provided that* $h \gg J$ and $J > Z/2$. The reason for these inequalities will become clear next.

We will be interested in states $|\downarrow\uparrow\downarrow\rangle$ and $|\downarrow\downarrow\downarrow\rangle$ since these are the two relevant states when $A=B=0$ (i.e., both peripheral dots have downspin polarization). The ground state and the fifth excited eigenstate in Table I contain state $|\downarrow\uparrow\downarrow\rangle$, while the first excited eigenstate is purely $|\downarrow\downarrow\downarrow\rangle$ with no other state mixed in. The ground state and the fifth excited eigenstate are entangled states and neither is purely $|\downarrow\uparrow\downarrow\rangle$.

We can make the ground state approach the pure unentangled state $|\downarrow\uparrow\downarrow\rangle$ if we make $|\alpha_1/2J| \gg 1$, i.e., if $h \gg J$. In order to make the fifth excited eigenstate approach the unentangled state $|\downarrow\uparrow\downarrow\rangle$, we need to make $|\alpha_6/2J| \gg 1$, but this is unachievable by any means. Therefore, if we make $h \gg J$, then the ground state is approximately state $|\downarrow\uparrow\downarrow\rangle$ and the first excited state is state $|\downarrow\downarrow\downarrow\rangle$. The energy difference between these two states is $4J-2Z$. Consequently, when $A=B=0$, the energy splitting between the three-body states corresponding to opposite spin polarizations in dot **C** (which is

TABLE I. Eigenenergies and eigenstates when the inputs $[A,B]$ are $[0,0]$. $\Delta_1 = \sqrt{(h+J)^2+8J^2}$, $\Delta_2 = \sqrt{(h-J)^2+8J^2}$, $\alpha_1 = -J-h-\Delta_1$, $\alpha_3 = J-h+\Delta_2$, $\alpha_6 = -J-h+\Delta_1$, $\alpha_7 = J-h-\Delta_2$, and $\beta_n = \sqrt{(\alpha_n/J)^2+8}$.

Eigenenergies (E_n)	Eigenstates (ψ_n)
$-J-h-Z-\Delta_1$	$[0,\ 2/\beta_1,\ \alpha_1/(J\beta_1),\ 0,\ 2/\beta_1,\ 0,\ 0,\ 0]$
$2J-2h-3Z$	$[1,\ 0,\ 0,\ 0,\ 0,\ 0,\ 0,\ 0]$
$-J+h+Z-\Delta_2$	$[0,\ 0,\ 0,\ 2/\beta_3,\ 0,\ -\alpha_3/(J\beta_3),\ 2/\beta_3,\ 0]$
$-Z$	$[0,\ \frac{1}{\sqrt{2}},\ 0,\ 0,\ -\frac{1}{\sqrt{2}},\ 0,\ 0,\ 0]$
Z	$[0,\ 0,\ 0,\ -\frac{1}{\sqrt{2}},\ 0,\ 0,\ \frac{1}{\sqrt{2}},\ 0]$
$-J-h-Z+\Delta_1$	$[0,\ 2/\beta_6,\ \alpha_6/(J\beta_6),\ 0,\ 2/\beta_6,\ 0,\ 0,\ 0]$
$-J+h+Z+\Delta_2$	$[0,\ 0,\ 0,\ 2/\beta_7,\ 0,\ -\alpha_7/(J\beta_7),\ 2/\beta_7,\ 0]$
$2J+2h+3Z$	$[0,\ 0,\ 0,\ 0,\ 0,\ 0,\ 0,\ 1]$

TABLE II. Eigenenergies and eigenstates when the inputs are [1,1]; $h_A = h_B = -h < 0$. .

Eigenenergies	Eigenstates
$-J-h+Z-\Delta_1$	$[0, 0, 0, 2/\beta_1, 0, \alpha_1/(J\beta_1), 2/\beta_1, 0]$
$2J-2h+3Z$	$[0, 0, 0, 0, 0, 0, 0, 1]$
$-J+h-Z-\Delta_2$	$[0, 2/\beta_3, -\alpha_3/(J\beta_3), 0, 2/\beta_3, 0, 0, 0]$
$-Z$	$[0, -\frac{1}{\sqrt{2}}, 0, 0, \frac{1}{\sqrt{2}}, 0, 0, 0]$
Z	$[0, 0, 0, -\frac{1}{\sqrt{2}}, 0, 0, \frac{1}{\sqrt{2}}, 0]$
$-J-h+Z+\Delta_1$	$[0, 0, 0, 2/\beta_6, 0, \alpha_6/(J\beta_6), 2/\beta_6, 0]$
$-J+h-Z+\Delta_2$	$[0, 2/\beta_7, -\alpha_7/(J\beta_7), 0, 2/\beta_7, 0, 0, 0]$
$2J+2h-3Z$	$[1, 0, 0, 0, 0, 0, 0, 0]$

the energy difference between states $|\downarrow\downarrow\downarrow\rangle$ and $|\downarrow\uparrow\downarrow\rangle$) is

$$\hbar\omega_{AB} = \hbar\omega_{00} = 4J - 2Z. \tag{1}$$

This energy difference is positive as long as $J > Z/2$. In other words, state $|\downarrow\uparrow\downarrow\rangle$ is lower in energy than state $|\downarrow\downarrow\downarrow\rangle$ if the exchange coupling strength $2J$ is larger than one-half of the Zeeman splitting energy $2Z$ caused by the global magnetic field. Because of the stronger exchange coupling, which tends to orient spins in neighboring dots along antiparallel directions, the spin in dot **C** prefers to be aligned antiparallel to the global magnetic field (lower energy state).

Case II: $h_A = h_B = -h$: This is the case when $A = B = 1$. The eigenenergies and eigenstates are shown in Table II. They are obtained by replacing h with $-h$ in Table I.

The two states of interest when $A = B = 1$ are $|\uparrow\downarrow\uparrow\rangle$ and $|\uparrow\uparrow\uparrow\rangle$, which correspond to upsin polarizations in the peripheral dots. Once again, the ground state and the fifth excited eigenstate contain state $|\uparrow\downarrow\uparrow\rangle$ and the first excited eigenstate is purely state $|\uparrow\uparrow\uparrow\rangle$. The ground state and the fifth excited eigenstate are entangled states. We can make the ground state approach the pure unentangled state $|\uparrow\downarrow\uparrow\rangle$ if we make $h \gg J$, but we could never make the fifth excited eigenstate approach the unentangled state $|\uparrow\downarrow\uparrow\rangle$. In other words, if we apply strong enough input signals to dots **A** and **B** such that $h \gg J$, then the first excited eigenstate is state $|\uparrow\uparrow\uparrow\rangle$ and the ground state is state $|\uparrow\downarrow\uparrow\rangle$. The energy difference between these two states is $4J + 2Z$. Consequently, when $A = B = 1$, the energy splitting between upspin and downspin states in dot **C** is

$$\hbar\omega_{11} = 4J + 2Z. \tag{2}$$

In this case, the spin in dot **C** tends to align along the global magnetic field since the exchange interaction and Zeeman splitting act in concert, while in the previous case, they opposed each other. Exchange had won since it was stronger and made the spin in dot **C** preferentially orient itself against the global magnetic field.

Case III: $-h_A = h_B = h$: This is the case when $A = 1$, $B = 0$. The eigenenergies and eigenstates are shown in Table III.

The states of interest in this case are $|\uparrow\downarrow\downarrow\rangle$ and $|\uparrow\uparrow\downarrow\rangle$. The ground state is an entangled state, but it approaches the pure unentangled state $|\uparrow\downarrow\downarrow\rangle$ if we make $h \gg J$. Similarly, we can make the entangled first excited state approach the unentangled state $|\uparrow\uparrow\downarrow\rangle$ if we make $h \gg J$. In other words, if we apply strong inputs signals, i.e., strong local magnetic fields to align the spins in dots **A** and **B**, such that $h \gg J$, then the first excited eigenstate is approximately the unentangled state $|\uparrow\uparrow\downarrow\rangle$ and the ground state is the unentangled state $|\uparrow\downarrow\downarrow\rangle$. The energy difference between these two states is $2Z$. Consequently, when the inputs are $A = 1$ and $B = 0$, the energy splitting between the upspin and downspin states in dot **C** is

$$\hbar\omega_{10} = 2Z. \tag{3}$$

Case IV: $-h_A = h_B = -h$: This is the case when $A = 0$, $B = 1$. The eigenenergies are the same as in Table III since these energies depend on h^2 and are therefore insensitive to the sign of h. However, the eigenstates change since they depend on h. The new eigenstates are found by replacing $\pi_p^{(q)}$ with $\hat{\pi}_p^{(q)}$ ($p = 1-4$, $q = 1-8$), where

$$\hat{\pi}_p^{(q)}(h) = \pi_p^{(q)}(-h). \tag{4}$$

We can show following the previous procedure that

$$\hbar\omega_{01} = 2Z. \tag{5}$$

Thus, in the end, we have a situation whereby

$$\omega_{11} \neq \omega_{00}, \omega_{01}, \omega_{10}. \tag{6}$$

This is all we need for the dynamics of the TF gate.

TABLE III. Eigenenergies and eigenstates when the inputs are [0,1]; $-h_A = h_B = h > 0$. $\theta_1 = J[9(h/J)^2 - 10 + 3i\sqrt{3(h/J)^6 + 12(h/J)^4 + 69(h/J)^2 + 27}]^{1/3}$, $\theta_2 = -(4J^2/3\theta_1)[(h/J)^2 + 7/3]$, $\theta_3 = 2\theta_1/3 + 3\theta_2/2 = 2i\,\mathrm{Im}(2\theta_1/3)$, $\theta_4 = 2\theta_1/3 - 3\theta_2/2 = 2\,\mathrm{Re}(2\theta_1/3)$, $\pi_1^{(1)} = -\theta_4/2 - 2J/3 + 2h + (\sqrt{3}i/2)\theta_3$, $\pi_2^{(1)} = -\theta_4/2 - 2J/3 - Z + (\sqrt{3}i/2)\theta_3$, $\pi_3^{(1)} = [\pi_2^{(1)}]^2 + 2\pi_2^{(1)}(Z + J + h) + 4Jh + 2JZ - 4J^2 + Z^2 + 2hZ$, $\pi_1^{(2)} = \pi_1^{(1)}$, $\pi_2^{(2)} = \pi_1^{(1)} + 2Z$, $\pi_3^{(2)} = [\pi_2^{(2)}]^2 + 2\pi_2^{(2)} \times (-Z + J + h) + 4Jh - 2JZ - 4J^2 + Z^2 - 2hZ$, $\pi_1^{(3)} = \pi_1^{(1)} - \sqrt{3}i\theta_3$, $\pi_2^{(3)} = \pi_2^{(1)} - \sqrt{3}i\theta_3$, $\pi_3^{(3)} = [\pi_2^{(3)}]^2 + 2\pi_2^{(3)}(Z + J + h) + 4Jh + 2JZ - 4J^2 + Z^2 + 2hZ$, $\pi_1^{(4)} = \pi_1^{(2)} - \sqrt{3}i\theta_3$, $\pi_2^{(4)} = \pi_2^{(2)} - \sqrt{3}i\theta_3$, $\pi_3^{(4)} = [\pi_2^{(4)}]^2 + 2\pi_2^{(4)} \times (-Z + J + h) + 4Jh - 2JZ - 4J^2 + Z^2 - 2hZ$, $\pi_1^{(7)} = \theta_4 - 2J/3 + 2h$, $\pi_2^{(7)} = \theta_4 - 2J/3 - Z$, $\pi_3^{(7)} = [\pi_2^{(7)}]^2 + 2\pi_2^{(7)}(Z + J + h) + 4Jh + 2JZ - 4J^2 + Z^2 + 2hZ$, $\pi_1^{(8)} = \pi_1^{(7)}$, $\pi_2^{(8)} = \pi_2^{(7)} + 2Z$, $\pi_3^{(8)} = [\pi_2^{(8)}]^2 + 2\pi_2^{(8)} \times (-Z + J + h) + 4Jh - 2JZ - 4J^2 + Z^2 - 2hZ$, $\pi_4^{(n)} = [[\pi_3^{(n)}]^2/J^4 + 4[\pi_1^{(n)}]^2/J^2 + 16]^{1/2}$ $(n = 1-8)$.

Eigenenergies	Eigenstates
$-\theta_4 - 2J/3 - Z + \sqrt{3}i/2\theta_3$	$[0, \pi_3^{(1)}/(J^2\pi_4^{(1)}), 2\pi_1^{(1)}/(J\pi_4^{(1)}), 0, 4/\pi_4^{(1)}, 0, 0, 0]$
$-\theta_4 - 2J/3 + Z + \sqrt{3}i/2\theta_3$	$[0, 0, 0, \pi_3^{(2)}/(J^2\pi_4^{(2)}), 0, 2\pi_1^{(2)}/(J\pi_4^{(2)}), 4/\pi_4^{(2)}, 0]$
$-\theta_4 - 2J/3 - Z - \sqrt{3}i/2\theta_3$	$[0, \pi_3^{(3)}/(J^2\pi_4^{(3)}), 2\pi_1^{(3)}/(J\pi_4^{(3)}), 0, 4/\pi_4^{(3)}, 0, 0, 0]$
$-\theta_4 - 2J/3 + Z - \sqrt{3}i/2\theta_3$	$[0, 0, 0, \pi_3^{(4)}/(J^2\pi_4^{(4)}), 0, 2\pi_1^{(4)}/(J\pi_4^{(4)}), 4/\pi_4^{(4)}, 0]$
$2J - 3Z$	$[1, 0, 0, 0, 0, 0, 0, 0]$
$2J + 3Z$	$[0, 0, 0, 0, 0, 0, 0, 1]$
$\theta_4 - 2J/3 - Z$	$[0, \pi_3^{(7)}/(J^2\pi_4^{(7)}), 2\pi_1^{(7)}/(J\pi_4^{(7)}), 0, 4/\pi_4^{(7)}, 0, 0, 0]$
$\theta_4 - 2J/3 + Z$	$[0, 0, 0, \pi_3^{(8)}/(J^2\pi_4^{(8)}), 0, 2\pi_1^{(8)}/(J\pi_4^{(8)}), 4/\pi_4^{(8)}, 0]$

III. DYNAMICS OF THE TF GATE

The TF gate is realized if the spin in dot **C** toggles only when $A = B = 1$, and not otherwise. To achieve this, we utilize Rabi oscillations.[17–19] A rotating ac magnetic field is applied in the x-y plane, which has an angular frequency of rotation equal to ω_{11}. This field will flip the spin in dot **C** *only* when $A = B = 1$, by virtue of the inequality in Eq. (6). This realizes the TF gate. Note that the spin in dot **C** undergoes a transition by coherently emitting or absorbing a photon from the ac magnetic field. No energy dissipation takes place, consistent with the reversible nature of the TF gate.

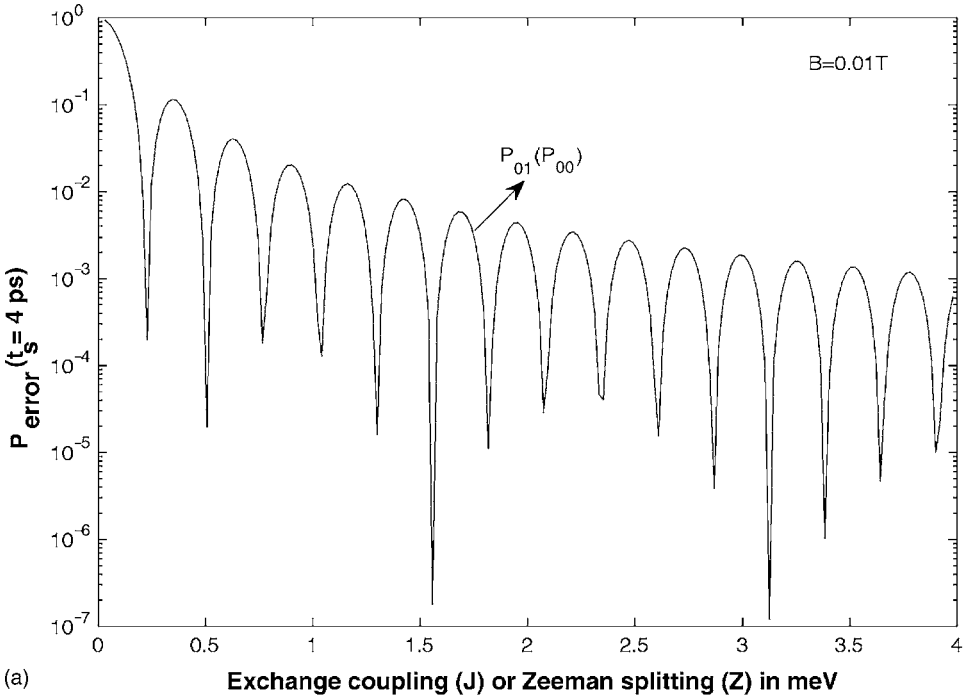

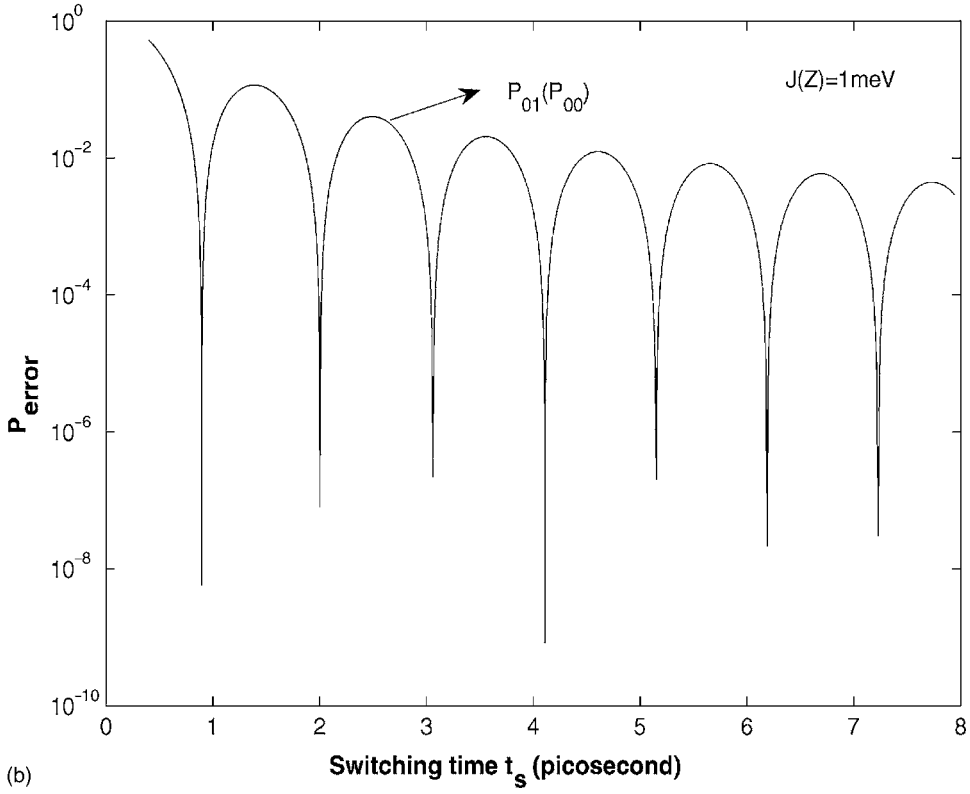

FIG. 2. (a) Gate error probability $P^{00}_{\text{error}}(t_s)$ and $P^{01}_{\text{error}}(t_s)[=P^{10}_{\text{error}}(t_s)]$ as a function of the Zeeman splitting Z or exchange coupling J for ac magnetic flux density amplitude of 0.01 T (t_s =4 ps) and (b) the same error probabilities plotted as a function of the switching time t_s when $J=Z=1$ meV.

The switching time is determined by the amplitude of the ac magnetic field B_{ac}. It is given by[17–19]

$$t_s = \frac{h}{2g\mu_B B_{\text{ac}}},$$

where g is the g-factor of the quantum dot material, h is the Planck constant, and μ_B is the Bohr magneton. The switching speed increases with increasing g-factor. A giant g-factor with an absolute value larger than 900 has been reported in $InSb_{1-x}N_{1-x}$.[20] With such large g-factors, the switching time is 4 ps with a reasonable $B_{\text{ac}}=0.01$ T. This is sufficiently fast.

The ac magnetic field is turned on only for the duration t_s given by the above expression. Such an ac magnetic field pulse is called a π-pulse.

IV. GATE ERROR

When the frequency of the ac magnetic field is resonant with ω_{11}, the probability of flipping the spin in dot **C** is

100% when $A=B=1$. However, it is not zero when either A or B, or both, is 0. If the spin flips when either A or B, or both, is 0, then we have a gate error. The probability of nonresonant Rabi spin flip, which is the gate error probability, is[17–19]

$$P(t)_{\text{nonresonant}} = P_{\text{error}}(t) = \frac{\omega_1^2/2}{\omega_1^2 + [\omega_{11} - \omega]^2}\{1 - \cos[t\sqrt{(\omega - \omega_{11})^2 + \omega_1^2}]\},$$

where t is the duration during which the ac magnetic field is kept on, $\omega_1 = g\mu_B B_{\text{ac}}/\hbar$, and $\omega = \omega_{00}$ or ω_{01} or ω_{10}.

In Fig. 2, we plot $P_{\text{error}}(t_s)$ for three cases: (i) $A=B=0$, (ii) $A=1$, $B=0$, and (iii) $A=0$, $B=1$. There is no difference between the last two cases.

The error probability $P_{\text{error}}(t_s)$ decreases with increasing difference $|\omega_{11}-\omega|$. Note that $|\omega_{11}-\omega_{00}|=4Z$ and $|\omega_{11}-\omega_{01}|=4J$. Therefore, in Fig. 2(a), we plot $P^{00}_{\text{error}}(t_s)$ as a function of Z and $P^{01}_{\text{error}}(t_s)$ $[=P^{10}_{\text{error}}(t_s)]$ as a function of J, for $B_{\text{ac}}=0.01$ T ($t_s=4$ ps). The error probability oscillates, but the envelope decays monotonically with increasing J. When $J \geq 1$ meV, or $Z \geq 1$ meV, the error probability falls below 0.03.

The error probability should also decrease if we decrease ω_1 and, therefore, B_{ac} (thus increasing t_s). The penalty incurred in doing this is a slower switching speed. Thus, there is a tradeoff between the switching speed and gate error probability. In Fig. 2(b), we plot $P^{00}_{\text{error}}(t_s)$ and $P^{01}_{\text{error}}(t_s)$ $[=P^{10}_{\text{error}}(t_s)]$ as a function of t_s for $J=Z=1$ meV. This value of J is realistic for semiconductor quantum dots.[21] For molecular systems, the value of J can be as high as 6 meV.[22] Once again, the error probability oscillates, but the envelope decays monotonically with increasing switching delay. When $t_s \geq 4$ ps, the error probability falls below 0.03.

There is no inherent error correction capability in reversible gates since there is no dissipation. Any error correction, if necessary, must be achieved with "software," using error correction algorithms. It has been recently shown that the most sophisticated error correction algorithms can correct errors occurring with probability up to 0.03.[23] Therefore, the fact that the error probability remains below 0.03 for reasonable values of parameters is immensely reassuring and raises hopes that spintronic TF gates will be achievable in the near term.

Before we conclude, let us estimate the strengths of the global dc magnetic field and the local magnetic fields that we need to write control bits A and B. Since $Z < 2J$ and $J=1$ meV, the global magnetic flux density $B_{\text{global}} < 0.04$ T if $g=900$. The strength of the local magnetic field is dictated by the requirement that $h \gg J$. How large should the ratio h/J be for the TF gate to work as described here? It turns out that it is adequate to have $h/J \geq 10$.[24]

Therefore, if the strength of the global magnetic field is 0.04 T, the strengths of the local magnetic fields required to write control bits A and B need not exceed 0.4 T. Fields of this strength can be easily generated on a chip.

V. CONCLUSION

In conclusion, we have presented a concrete scheme for the realization of a reversible spintronic TF gate. Single spin realization of irreversible single spin gates (e.g., NAND gate) has been proposed before,[25] but to our knowledge, this is the first concrete proposal for a reversible TF gate based on single spins. Using high g-factor materials, the switching speed can be made fast (few picoseconds). The gate error probability is within the handling capability of modern error correction algorithms.

[1] E. Fredkin and T. Toffoli, Int. J. Theor. Phys. **21**, 219 (1982).
[2] R. Landauer, IBM J. Res. Dev. **5**, 183 (1961).
[3] P. Benioff, Phys. Rev. Lett. **48**, 1581 (1982).
[4] R. P. Feynman, Int. J. Theor. Phys. **21**, 467 (1982).
[5] W. H. Zurek, Phys. Rev. Lett. **53**, 391 (1984).
[6] A. Peres, Phys. Rev. A **32**, 3266 (1985).
[7] See, for example, U. Sakaguchi, H. Ozawa, and T. Fukumi, Phys. Rev. A **61**, 042313 (2000).
[8] S. Bandyopadhyay and V. P. Roychowdhury, Superlattices Microstruct. **22**, 411 (1997).
[9] D. Loss and D. DiVincenzo, Phys. Rev. A **57**, 120 (1998).
[10] S. Bandyopadhyay, Phys. Rev. B **61**, 13813 (2000).
[11] T. Calarco, A. Datta, P. Fedichev, E. Pazy, and P. Zoller, Phys. Rev. A **68**, 012310 (2003).
[12] S. Muto, H. Sasakura, S. Adachi, Y. Kajiwara, and K. Shiramine, Physica E (Amsterdam) **13**, 616 (2002).
[13] F. L. Carter, *Molecular Electronics* (Dekker, New York, 1982); *Molecular Electronics II* (Dekker, New York, 1987).
[14] K. Obermayer, W. G. Teich, and G. Mahler, Phys. Rev. B **37**, 8096 (1988); W. G. Teich and G. Mahler, Phys. Rev. A **45**, 3300 (1992).
[15] S. Lloyd, Science **261**, 1569 (1993).
[16] S. N. Molotkov and S. S. Nazin, JETP Lett. **62**, 256 (1995); Phys. Low-Dimens. Semicond. Struct. **10**, 85 (1997).
[17] I. I. Rabi, Phys. Rev. **49**, 324 (1936).
[18] I. I. Rabi, Phys. Rev. **51**, 652 (1937).
[19] I. I. Rabi, N. F. Ramsey, and J. Schwinger, Rev. Mod. Phys. **26**, 167 (1954).
[20] X. W. Zhang, W. J. Fan, S. S. Li, and J. B. Xia, Appl. Phys. Lett. **90**, 193111 (2007).
[21] D. V. Melnikov and J.-P. Leburton, Phys. Rev. B **73**, 155301 (2006).
[22] C. F. Hirjibehedin, C. P. Lutz, and A. J. Heinrich, Science **312**, 1021 (2006).
[23] E. Knill, Nature (London) **434**, 39 (2005).
[24] H. Agarwal, S. Pramanik, and S. Bandyopadhyay, New J. Phys. **10**, 015001 (2008).
[25] S. Bandyopadhyay, B. Das, and A. E. Miller, Nanotechnology **5**, 113 (1994).